Seismic refraction methodology for groundwater level determination: "Water seismic index"

Article *in* Journal of Applied Geophysics · July 2009

DOI: 10.1016/j.jappgeo.2009.02.001

2 authors:

Gerardo Grelle
Sapienza University of Rome
82 PUBLICATIONS **618** CITATIONS
SEE PROFILE

Francesco M. Guadagno
Università degli Studi del Sannio
159 PUBLICATIONS **1,791** CITATIONS
SEE PROFILE

Journal of Applied Geophysics 68 (2009) 301–320

Contents lists available at ScienceDirect

Journal of Applied Geophysics

journal homepage: www.elsevier.com/locate/jappgeo

Seismic refraction methodology for groundwater level determination: "Water seismic index"

Gerardo Grelle *, Francesco Maria Guadagno

Department of Geological and Environmental Studies, University of Sannio, Benevento, Italy

ARTICLE INFO

Article history:
Received 10 October 2008
Accepted 3 February 2009

Keywords:
Body waves
Seismic refraction tomography
Water table

ABSTRACT

Recently, there has been increased interest in the use of refraction seismic data for the exploration and development of hydrological reservoirs. The aim of this study is to provide a procedure in order to identify groundwater levels by means of seismic refraction profiles. Assuming that the velocity of shear waves increases much less than the velocity of compressional waves in a saturated soil, seismic refraction surveys were performed for the determination of the water table. In order to have a perfect overlay of the tomography 2D grids, *P* and *S* wave seismic profiles were obtained with the same geometrical configuration. Based on the propagation of the *P* and *S* waves in the unsaturated and saturated media, a "Water Seismic Index" (WSI) was defined. WSI is related to the local variations of the *P* and *S* wave velocities and, in theoretical terms, it is correlated to groundwater level. Preliminary results indicate that there is a good agreement between the depth of the ground water and the WSI parameter.

1. Introduction

The relationship between lithological proprieties and body wave velocity has been explored, for many years, as a means of indirectly characterizing porous aquifers. In existing literature, different approaches have been proposed: in some cases the water table level is attributed to specific V_P values (Zohdy et al., 1974; Sander, 1978; Haeni, 1986; Hasselstroem, 1996); while in others, the hypothetical aquifer layer is identified via its V_P/V_S ratio (Stümpel et al., 1984; Castagna et al., 1985; Nicholson and Simposon, 1985) or Poisson's ratio (Lees and Wu, 2000). In addition, more complex theory-based approaches exists which derive from the principles of the elastic wave propagation within saturated and unsaturated porous media (Foti et al., 2002). These approaches require a preliminary and detailed knowledge of the lithological sequences of the site under investigation.

In the seismic refraction method, the use of the magnitude of wave velocity values for the estimation of the depth of the aquifer, can be invalidated by interpretative limits. In fact, case histories show a wide range of V_P values in connection to the water table level. In addition, these values are not uniquely correlated to the aquifer layer. Some authors attribute *P*-wave velocities around 1500 m/s to represent a saturated layer. Instead Hasselstroem (1969) proposes a *P*-wave velocity between 1200 and 1800 m/s in porous materials. This non-unique value of V_P is confirmed by Haeni (1986) for New England glacial materials. Tomographic studies show that the water table corresponds to a *P*-wave velocity of 1100–1200 m/s (Azaria et al., 2003; Zelt et al., 2006), with values as low as 1000 m/s (Watson et al., 2005).

Theoretical approaches demonstrate that in a sandy deposit, the maximum increase of V_P occurs at a water content corresponding to a saturated state, Sr = 1.00, where Sr is the degree of saturation (Biot, 1956a,b; 1962). Laboratory experiments (Yoshimi et al., 1989) show that "low saturation" in sand, is related to V_P significantly smaller than 1500 m/s. This is due to the fact that the attainment of this value is defined by the relationship $(1\text{-}Sr) < 10^{-5}$. In reference to the afore-mentioned, Bachrach and Nur (1998) highlight that in field investigations, reflections as well as refractions are influenced by the degree of saturation. In addition, they show how V_P is influenced by pore-water pressure.

The methodology presented in this paper, attempts to define an index parameter directly related to the depth of the water table. The "Water Seismic Index" (WSI) is theoretically derived from the propagation of elastic body waves in 2D or 3D spatial models of water table surfaces in unsaturated–saturated interfaces.

This study was carried out utilizing seismic refraction investigations to obtain the spatial distribution of V_P and V_S values. Field tests were performed in areas with known lithological and hydrogeological conditions.

2. Methodology

The refraction method is widely used for the characterization of groundwater depth. In particular, in porous soils, the unsaturated vs saturated interface, is a refracting surface, efficaciously detected by the afore-mentioned exploration method (Haeni, 1988). Lawton

* Corresponding author. Dipartimento di Studi Geologici ed Ambientali, Facoltà di Scienze MM. FF. NN. Università degli Studi del Sannio, via dei Mulini, 59/A-Palazzo Inarcassa, 82100 Benevento, Italy. Tel.: +39 0824 323650; fax: +39 0824 323623.
E-mail address: gerardo.grelle@unisannio.it (G. Grelle).

0926-9851/$ – see front matter © 2009 Elsevier B.V. All rights reserved.
doi:10.1016/j.jappgeo.2009.02.001

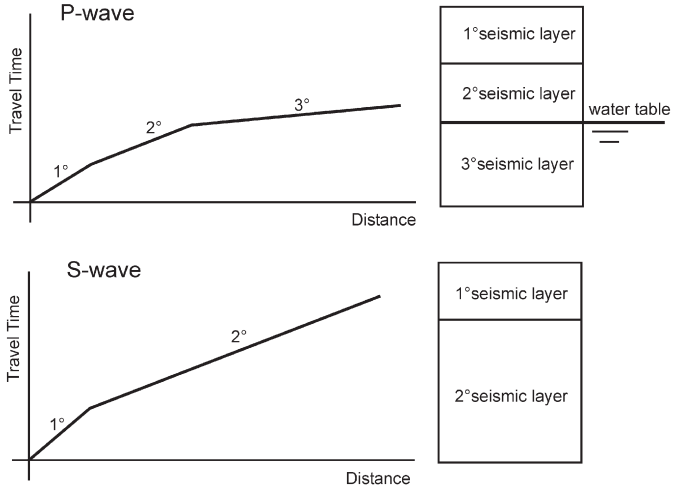

Fig. 1. *P*-wave and *S*-wave travel time patterns related to a multilayer sequence with water table presence.

(1990) compared V_P and V_S values of subsoil models obtained from seismic refraction tests. In some cases, he highlighted that the resulting higher number of V_P seismic-layers, was due to the presence of a groundwater table (Fig. 1).

The compressional-waves and shear-waves propagation modality, which was confirmed by field tests, indicates that V_P should increase at the transition from unsaturated to saturated layers. This transition zone does not seem to be influenced by V_S (Stümpel et al., 1984).

The "Water Seimic Index" (WSI) is an estimator parameter that was created in relation to these proprieties. It is defined by the equation:

$$\mathrm{WSI} = \left(\frac{z\delta V_P}{V_P}\right) \cdot \left[1 - \left(3\frac{z\delta V_S}{V_S}\right)\right]; \quad (1)$$

where V_P and V_S are, respectively, the compressional and shear waves velocity, expressed in m/s, and z is depth, expressed in m. The coefficient "3", discussed below, aims at giving a correct load to the V_S variability. In particular, it is correlated to the most recurrent values in the V_P/V_S ratio for granular soils in the near surfaces (Stümpel et al., 1984).

In synthesis, the WSI considers the combined local spatial distribution of V_P and V_{SH} values with depth; the objective is to obtain a parameter which is indicative of the presence and depth of the water table.

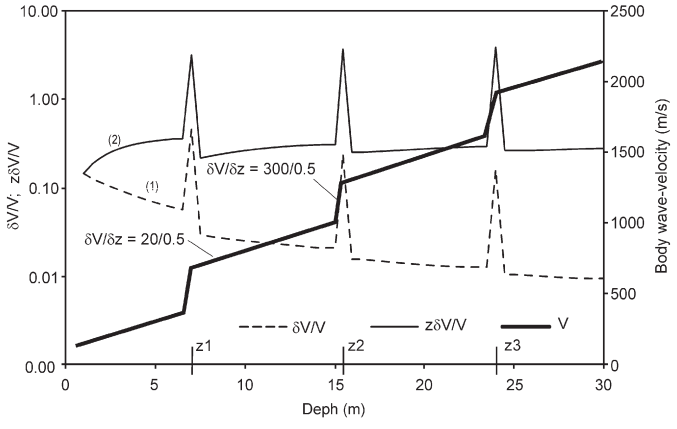

Fig. 2. Pattern of the generic variable function (1) and (2) in relation to velocity vs depth pattern.

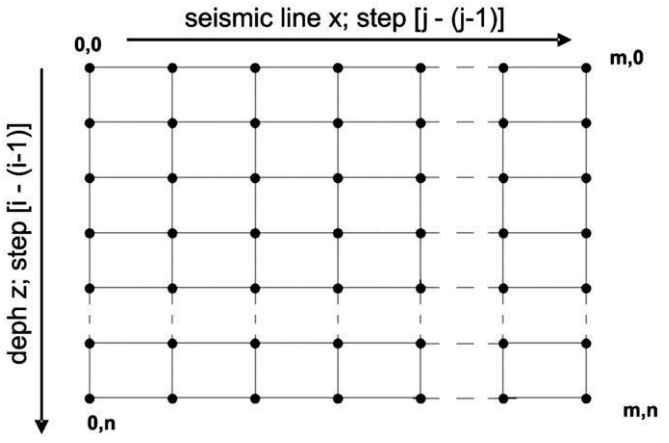

Fig. 3. Two-dimensional grid of the WSI distribution.

The WSI formulation takes into consideration the general increase of absolute body wave velocities in relation to depth. If this does not occur, a non-uniform response by the WSI along the depth direction, can result. Fig. 2, shows the pattern $\delta V/V$ of the generic variable ratio (1) and the corresponding normalized variable $z\delta V/V$ (2), in the condition of the $\delta V/\delta z$ gradient, which is positive and constant except for three points $z1$, $z2$ and $z3$ along the depth direction. Having imposed an elevated and equal value of δV around these points, curve (2), in contrast to curve (1), shows peaks which are similar to one another. The normalization operation led the WSI to be expressed by the surface dimensional unit.

The WSI formulation lends itself well to being interpreted via 2D or 3D tomography methodology. A bi-dimensional analysis requires that every node (i,j) must have overlapping $V_{P(i,j)}$ and $V_{SH(i,j)}$ values (Fig. 3) for an assigned x–z grid (x: seismic line direction and z: depth direction). In this context, the WSI is defined by the reciprocal local variation of the compressional and shear velocity along the z direction (i–1, i), for every×range (j–1, j). Therefore, the equation is:

$$\mathrm{WSI} = \left(\frac{z_{(i,j)}\left(V_{P(i,j)} - V_{P(i-1,j)}\right)}{V_{P(i,j)}}\right) \cdot \left[1 - \left(3\frac{z_{(i,j)}\left(V_{S(i,j)} - V_{S(i-1,j)}\right)}{V_{S(i,j)}}\right)\right] \quad (2)$$

in the condition that $(z_{(i,j)} - z_{(i-1,j)}) = \delta z$ is a constant. The more the effect of the δz grid value on the WSI increases, the greater is the gradient $\delta V/\delta z$ before and after the seismic layer variation. However, as shown in Fig. 4, the choice of different grid δz ranges determines the small variation of the $z\delta V/V$ peak and therefore of the WSI values,

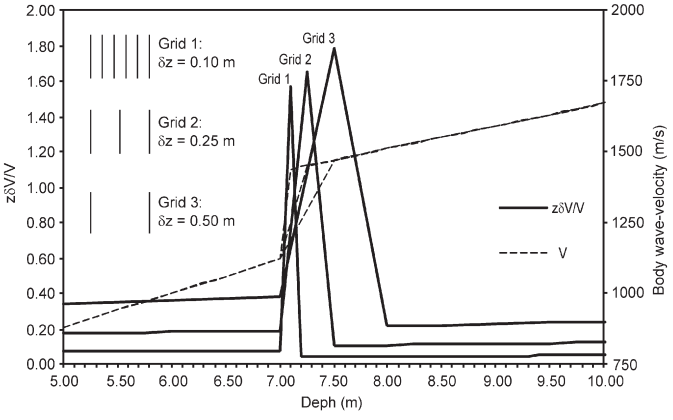

Fig. 4. Variation of the $\delta V/V$ in relation to the δz grid.

Table 1
Mathematical combination of the *P* waves and *S* waves velocity, in relation to lithology and hydrogeology transition and WSI value range results; where: ↑ increase; ↓ decrease; ↕ weak variation; $\varepsilon \sim 0$ and $\varepsilon < \varepsilon^* < \varepsilon_1$.

Relation	$\delta V_{P(i,j)} = (V_{P(i,j)} - V_{P(i-1,j)})$	$\delta V_{S(i,j)} = (V_{S(i,j)} - V_{S(i-1,j)})$	WSI range	Condition	Combinations
1	↕	↑↕↓	$[-\varepsilon,\varepsilon]$	Interbed or layer shift (rigidity variation)	3
2	↑	↑	$[-\varepsilon_1,\varepsilon]$	Layer shift	1
3	↓	↕↓↑	$[-\varepsilon_1,-\varepsilon]$	Layer shift (velocity inversion)	3
4	↑	↕↓	$[\varepsilon^*,\varepsilon_1]$	Water table presence	2

taking into consideration that the choice of the δz is suitably conditioned by the intergeophone distance.

The WSI is characterized by a finite domain, in which the values can be referable to particular lithological and hydrogeological conditions. In fact, in mathematical terms, the local independent variations of the δV_P and δV_{SH}, are characterized by the number of possible combinations equal to 3^2 (Table 1). Instead, taking into consideration the lithological and hydrogeological sequences which constitute the subsoil, fewer combinations are obtained. This is defined by the following WSI range values (Table 1):

i. close to zero, in relation to (1) small increase or decrease of the δV_P and δV_{SH} values, which correspond to the inter-layer condition, or (2) to the increase of both the δV_P and δV_{SH} values, which correspond to the lithological variation.
ii. negative, in relation to (3) the decrease of both the δV_P and δV_{SH} values, which correspond to the lithological variation characterized by an inversion seismic velocity of the layers.
iii. positive, in relation to (4) the univocal increase of the δV_P values, which correspond to the water table presence.

Additionally, interlayer conditions under the water table level are referable to the above-mentioned points, i. and ii. With regards to this subject, Fig. 5 shows the WSI behaviour in relationship to some 1D patterns of *P* and *S*-wave velocities which are hypothetically extracted from 2D seismic refraction tomography models.

Post-analysis processing was used in the following illustrated experimentation. In reference to Table 1, the aim of the tests was to provide two pieces of interdependent information. The first was the verification of the peak values of the WSI in connection to the depth-level of a known water table. The second was to determine the lower limit ε^* value which identifies the minimum positive value of the WSI in relation to the presence of the groundwater level.

3. Experimental areas

The seismic refraction tests were performed in three different locations, during the period June–July 2007. The geological sequences of these locations were known. Furthermore, it was possible to verify the water table depth using piezometers, installed at the site, during the field tests. The S1, S2 and S3 test-locations were situated in the southern Italian region of Campania's Appennines (Fig. 6). They were lowland-sites, and were characterized by granular soil and clay sequences, which are typical of alluvial valleys or, in general, to Plio–Quaternary natural-fills of ancient morphological depressions. In contrast to S1 and S2, the lithological sequence of S3 was characterized by a lateral and vertical heteropy between gravel–sands and clay (Giocoli et al., in press). Furthermore the three localities were characterized by overlapping pluriaquifers. The tests were performed in relation to the highest aquifers.

From the borehole prospecting performed, the three localities presented the following lithological sequences (Fig. 6):

S1 "Cubante Plain" site: piroclastic deposits on sand–gravels and silt–sands sustained by clay and stiff clay;
S2 "Dragone Valley" site: a thick piroclastic sequence characterized by thin interlayers of peat and fluvio-lacustrine deposits.
S3 "Ufita Valley" site: fluvio lacustrine deposits characterised, in the superior part of the sequence by sand and gravel sand with clay lenses, sustained by clay and boulder clay deposits. In particular, the highest aquifer, is fed by the Ufita River and is interconnected locally with the deeper aquifers.

4. Experimental procedure

In order to determine the travel times of *P*-waves and SH-waves, the seismic refraction tests were carried out by two overlapping linear arrays. These arrays were equipped with twenty-four vertical and horizontal mono-component geophones with a resonant frequency of 10 Hz. The horizontal geophones were orientated orthogonally to the seismic line; these geophones were equipped with a levelling bubble and an arrow for orientation. Time zero was established by a trigger geophone positioned near the sources.

Two different types of sources were used for *P*-waves and *S*-waves generation. Fig. 7 shows the scheme related to the disposition of the five sources along the arrays used in the tests. In particular, two sources were positioned externally to the most extreme geophones, at a distance which was equal to half the intergeophone distance. The other sources were positioned at the following distances: one at 1:4, one at 1:2 and one at 3:4 of the linear array. The intergeophone distances used were 2.00 m at the S1site, 2.50 m at the S2 site and 4.00 m at the S3 site.

The *P*-wave source consisted of a 10 kg steel hammer which struck against an aluminium plate. Great care was taken in the production and acquisition of SH-waves. The SH-waves were produced by a portable apparatus specifically built for the purpose. It consisted of a

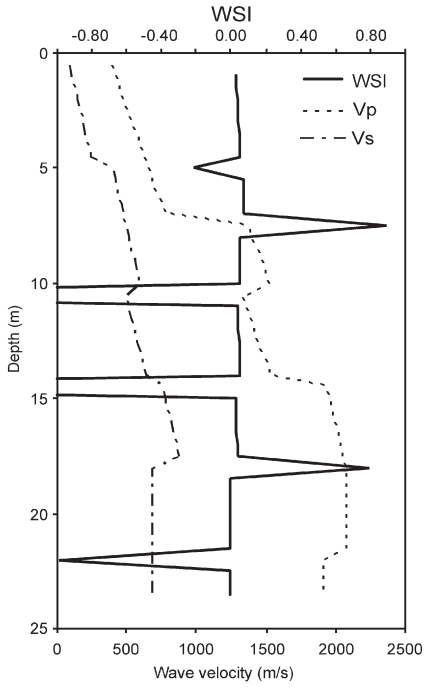

Fig. 5. 1D patterns of *P* and *S*-wave velocities which are hypothetically extracted from 2D seismic refraction tomography models.

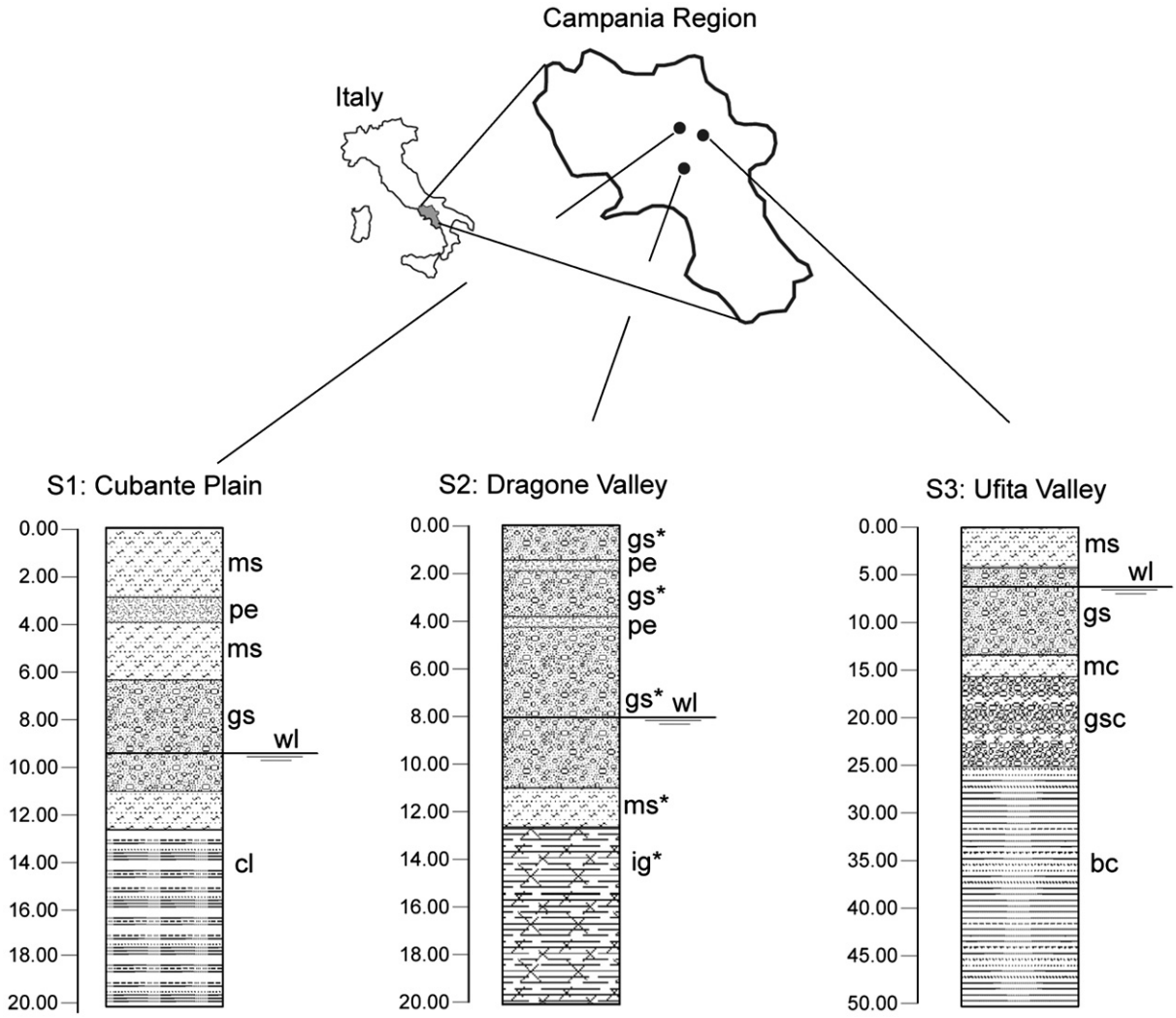

Fig. 6. Field tests sites and borehole lithology sequences; bc: clay with boulder; cl: clay and stiff clay; gs: gravely sand; gsc: gravely sand with clay layers; ig: "ignimbrite" tuff; mc: clayey silt; ms: sandy silt; pe: peat; wl: water level; (*) volcanic origin.

wooden block, weighed down for intimate contact, as shown in Fig. 8. The block was positioned with the length orthogonal to the seismic line. The shear waves were produced by the steel hammer which, in alternating movements, struck the lateral surface. *P* and *S* wave-field separation techniques were used to minimize the hidden or equivocal phenomena regarding the arrival of the first-breaks of the SH-wave (Hasbrouk, 1987). This technique consisted of multi-signal recording obtained from the subtraction (sum inverted) of the traces produced with inverse polarization. Fig. 9 shows the traces produced by the *P* wave source and the SH wave source and the related first breaks singled out for the S1 site.

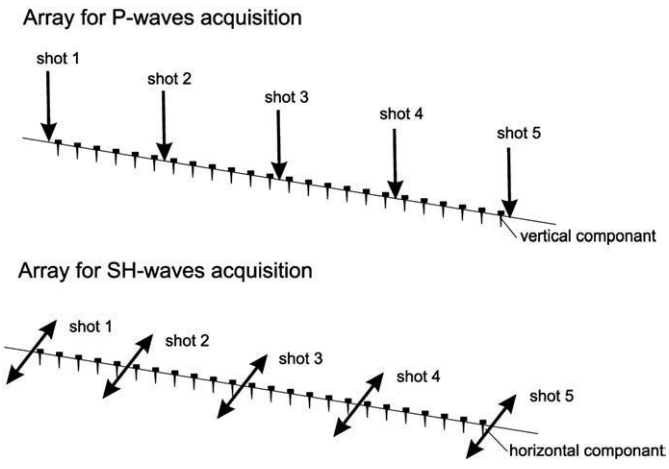

Fig. 7. Array and typology sources of the *P* and SH waves.

The V_P and V_{SH} 2D refraction tomography models were obtained via the Rayfract code. This is an inversion system based on "wavepath eikonal travel time" (WET) devised by Schuter and Quintus-Bosz (1993). This method utilizes a back-projection formula of finite differences based on the eikonal equation (Qin et al., 1992). The procedure foresees that an inversion routine adjusts the initial velocity model until an acceptable match between the calculated and measured first-arrival travel times is obtained. The initial velocity model is defined by a 1D gradient which is then extended to cover the two-dimensional area.

5. Results and discussion

Fig. 10 shows the 2D traveltime tomography of the *P* and SH velocity related to the S1, S2 and S3 arrays. An initial comparison between the compressional waves and the aquifer layers, highlights values ranging from 1200 to 1400 m/s for S3, in accordance with the results of Hasselstroem (1969) and Haeni (1986). In contrast, for the

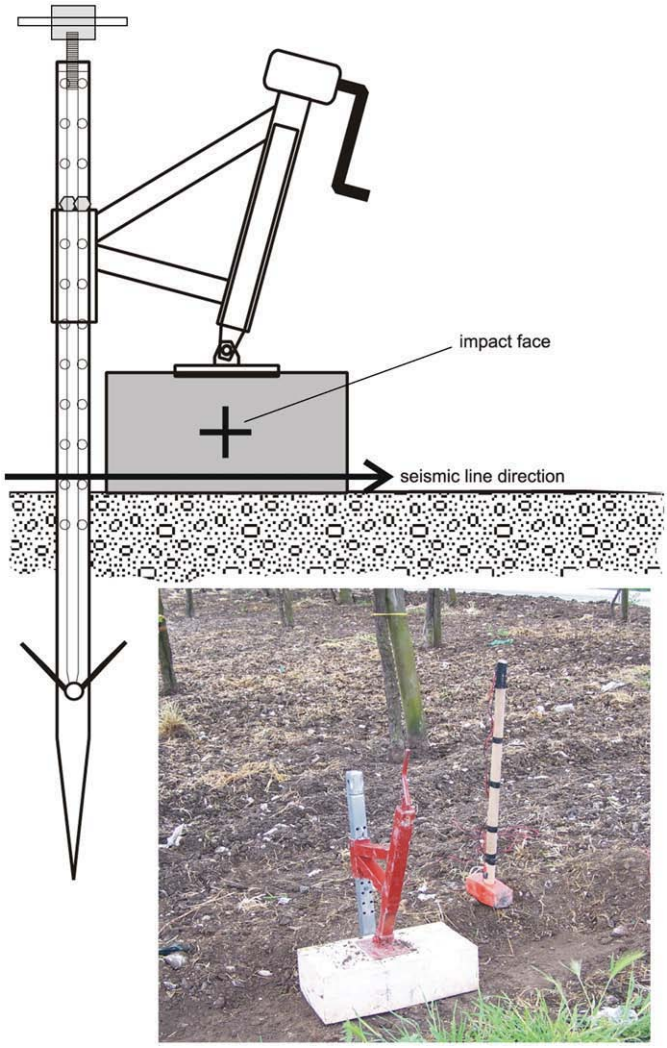

Fig. 8. Apparatus for SH waves generation.

S1 and S2 arrays, this velocity is close to or less than 1000 m/s. For these latter localities, the lithological sequences identified thin higher aquifer layers for which it was possible to hypothesize non-uniform saturated conditions.

A comparison between the theoretical (synthetic) and experimental first-arrival times (Fig. 11), highlights a fitting with an average residual time of less than 2.00 m/s, with the exception of the fitting related to the V_{SH} of S2 (with an average residual time of 8.09 m/s). In general terms, due to the combinatorial character of the Eq. (1), the WSI model error results as being connected to the greatest value between the average residual times of the V_P and V_{SH} spatial models. In addition, it is important to highlight that, in this context, the inverse problem of refraction travel time, as in many other geophysical investigation methods, can be affected by non-uniqueness model results (Ackerman et al., 1986; Ivanov et al., 2005).

The WSI one-dimensional analysis (Fig. 12), extracted from the WSI two-dimensional distribution, demonstrates how the peak values correspond to the presence of the water tables, for each experimental case. Furthermore, it highlights that $\varepsilon^* = 0.5$ can be considered as the threshold which indicates the existence of the water table.

Based on both the presuppositions reported in Table 1 and the established ε^* value, Fig. 13 illustrates the chromatic variation related to the WSI two-dimensional distribution for each experimental-site. In this context, the WSI water table models (WSI>0.5) are characterized by horizontally developed and near continuous areas.

The WSI spatial models can agree with the modality of the groundwater circulation. In particular:

- In site S1, the different depths resulting from the WSI water table model, is related to the non uniform lowering of the water table during the dry period. This induces a local and momentary suspension condition of the water table.
- In site S2, the WSI water table model primarily shows a uniform and horizontal distribution of the water table; this is in accordance with the water circulation in the aquifer layer.
- In site S3, the spatial distribution of the WSI seems to be concordant with groundwater circulation. In fact, as previously stated in this paper, the aquifer layer is characterized by lateral and vertical variations of granular soils and clay.

Studies, related to refraction seismic tests, have illustrated the variation of *P*-waves and *S*-waves velocity in granular soils and in clay. In particular, Stümpel et al. (1984) discussed the behaviour of the afore-mentioned velocities in dry and saturated conditions. Fig. 14 shows a high increase of V_P and an unchanged value of V_S between the dry and saturated sand. Inversely, the saturated clay shows both a greater ratio V_P/V_S and also greater values of V_S in comparison to saturated sand. Taking this into account, as well as the water circulation modality in granular soils and in clays, the spatial behaviour of the WSI can be characterised as follows:

i. In clays, the suction phenomenon determines a gradual variation of the water content during the transition between the upper zone and the lower zone of the water table. It involves lower δV_P values for suitable δz values. In contrast, the suction is weak in granular soils. This determines a greater propensity of the WSI for the investigation of water tables in such soils.
ii. The V_S increase during the transition from saturated sands to clay, and the V_S decrease in the inverse transition, determine two different behaviours of the WSI. In both cases, a fundamental role is provided by the ratio 1:3 between δV_P and δV_S (Eqs. (1) and (2)). In the first case, the WSI shows values close to zero, negative, or less than ε^*. In the second case the WSI shows positive values which can also exceed ε^*.

Bearing these observations in mind, it is possible to hypothesize that the WSI individualizes granular aquifers inside a saturated granular soil–clay sequence. In reference to site S3, Fig. 15 shows how the negative values of the WSI correspond to clayey sublayers inside the aquifer layer and to the clayey bed layer.

Fig. 16 highlights a greater variability of the WSI in relation to the V_P/V_{SH} and the dynamic Poisson's ratio. In particular, these last two parameters do not show any peak condition or evident increase of their pattern in correspondence to the water table.

6. Conclusions

The traditional parameters resulting from seismic refraction tests do not always provide exhaustive and above all unequivocal information about groundwater levels. The WSI formulation gives direct information both on the existence and on the level of the groundwater table. This is due to the fact that it is based on a different modality which regulates the propagation of the compressional and shear waves in the physical media. Furthermore, its mathematical form requires a spatial distribution of body wave velocity. This requires a tomography analysis of data and therefore a seismic refraction array related to the *P* and SH traveltime waves acquisition.

The application of the methodology in three areas permitted the determination of the positive minimal ε^* values of the WSI correlated to the groundwater level. In addition, the two-

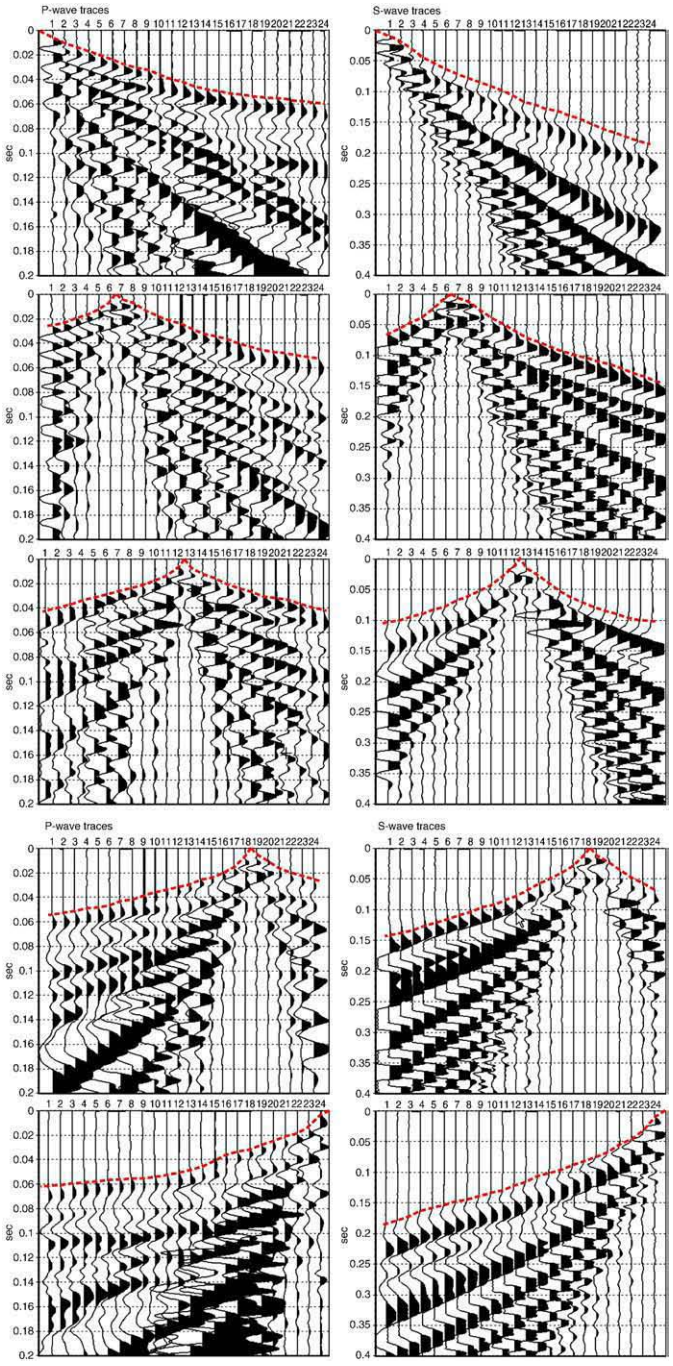

Fig. 9. Seismograph records and first-break selection of *P* and SH waves: resulting from S1 site tests.

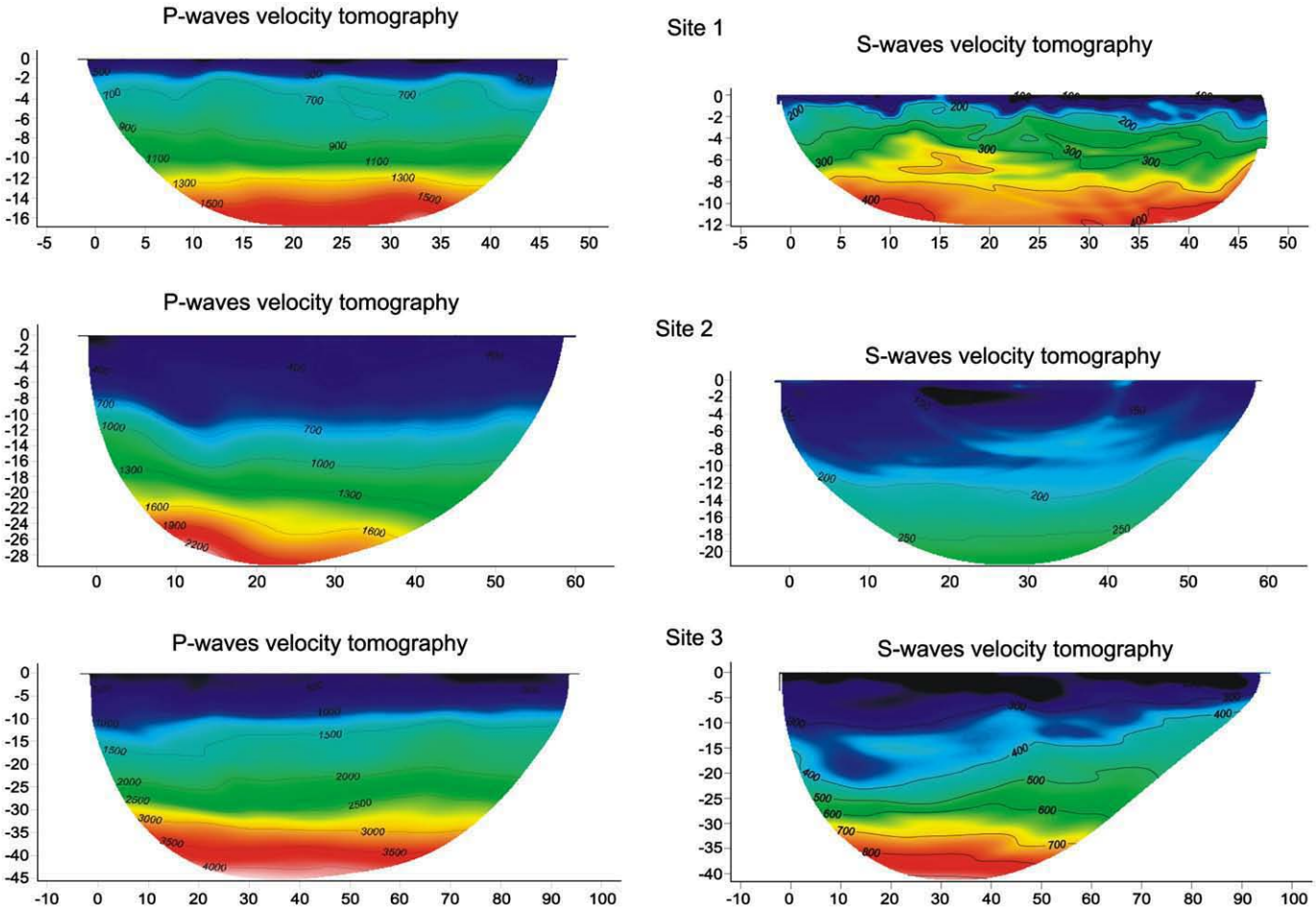

Fig. 10. Tomography2D models of *P* and SH waves velocity.

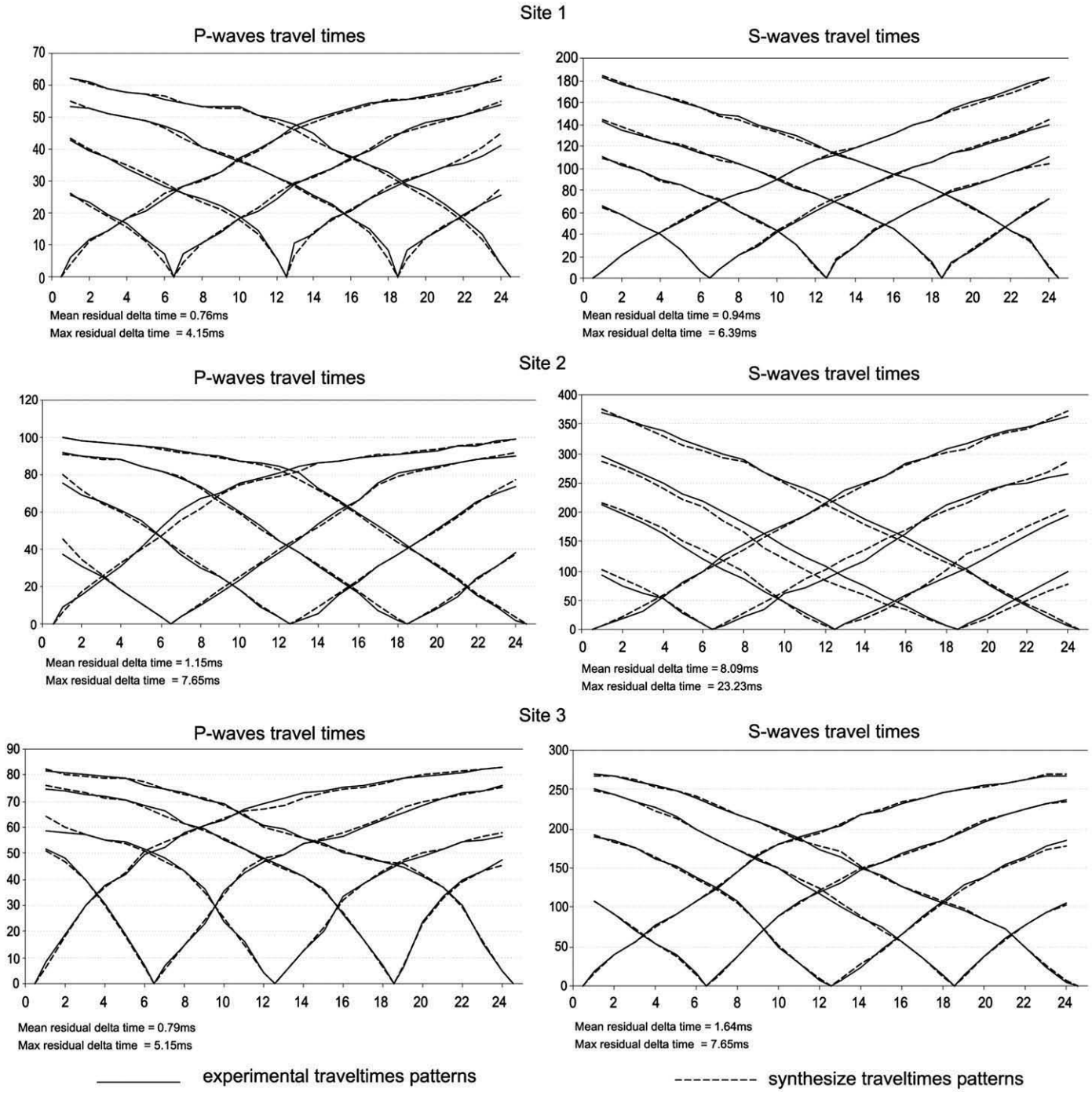

Fig. 11. Comparison between theoretical and experimental first-times for *P* and SH velocity models.

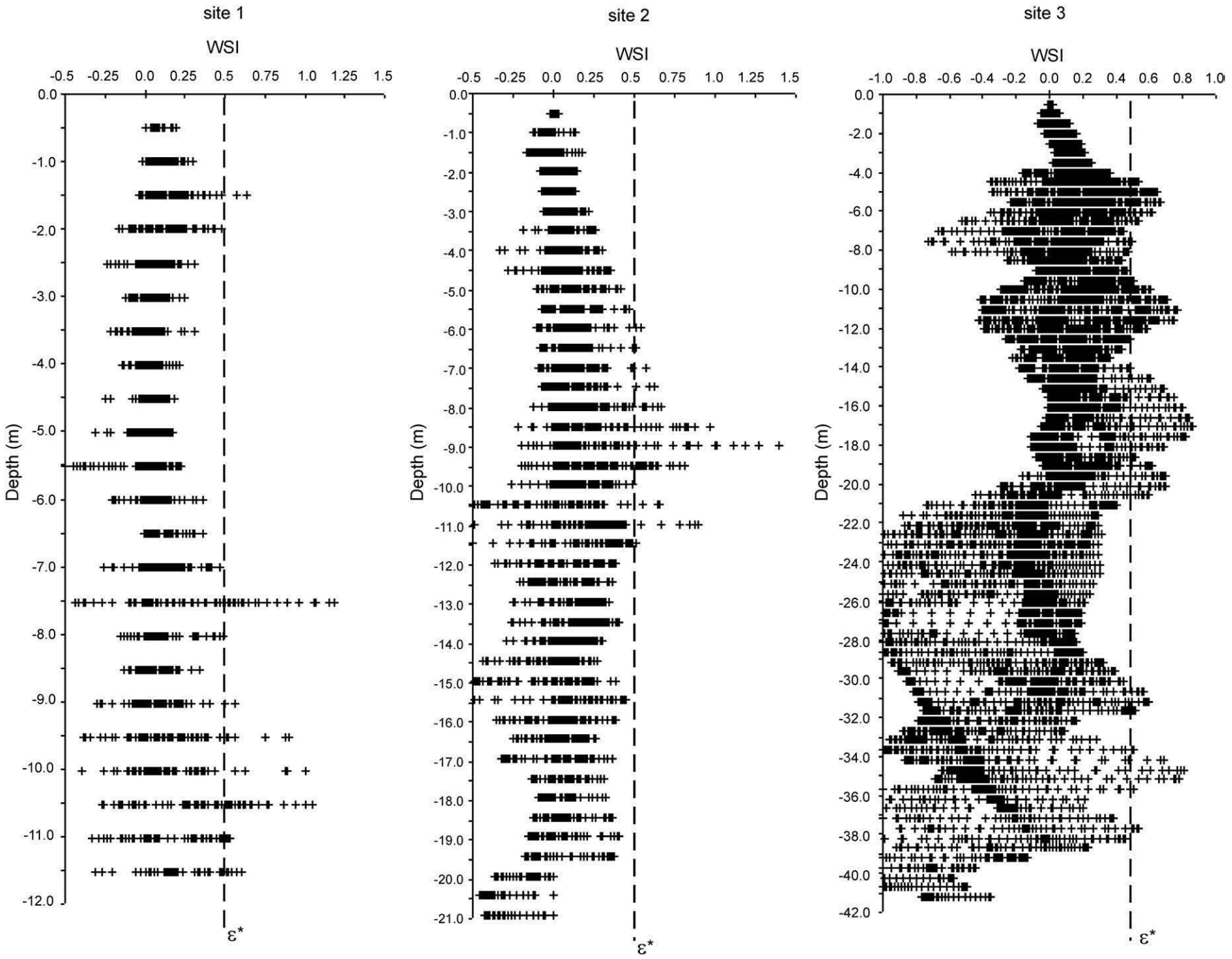

Fig. 12. WSI one-dimensional pattern and value of the minimal threshold index.

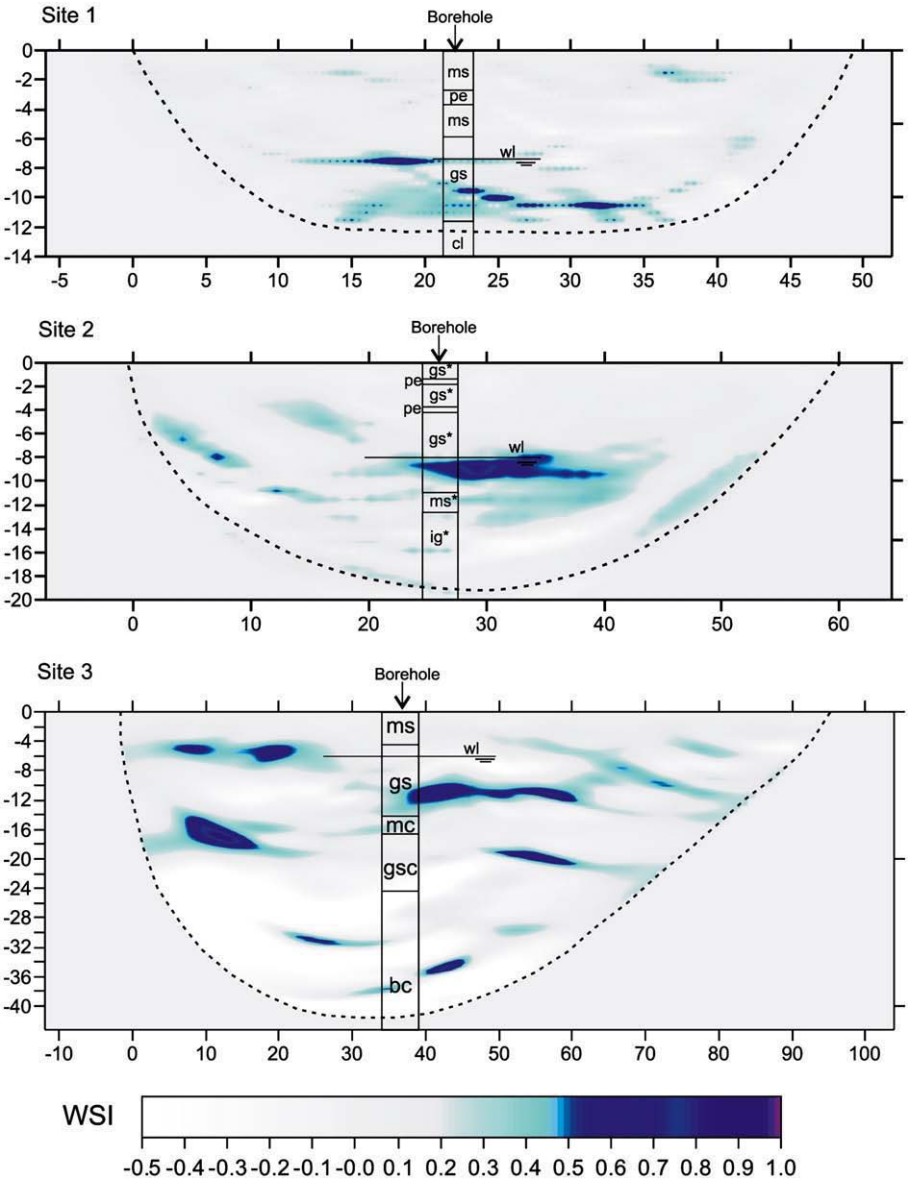

Fig. 13. WSI two-dimensional models (for soil suffixes see Fig. 6).

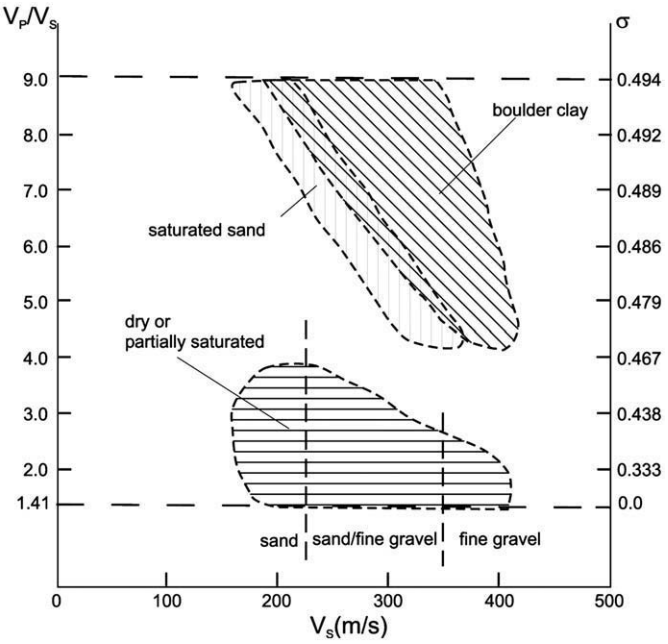

Fig. 14. V_P/V_S and Poisson's ratio (σ) versus V_S for some soils from in-situ measurements (modified by Stümpel et al., 1984).

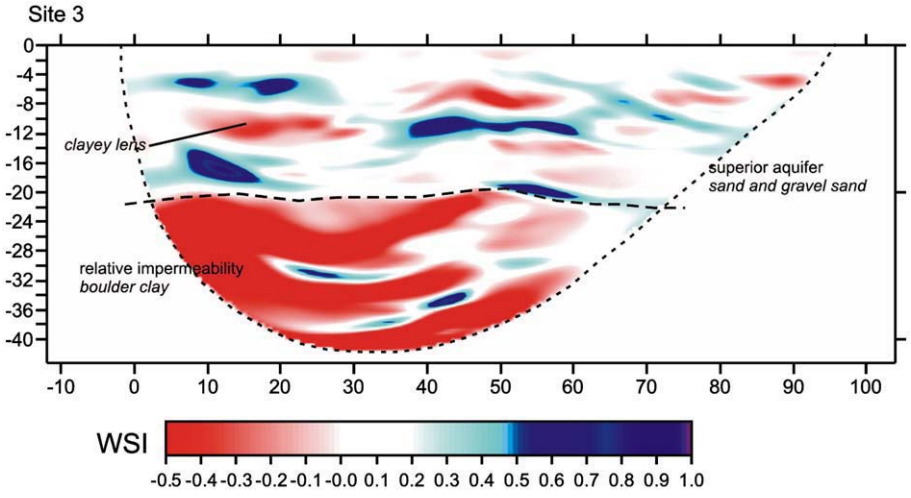

Fig. 15. Lithology and hydrogeology interpretation in relation to the WSI 2D distribution.

dimensional distribution of the WSI demonstrated that ε^* is exceeded only in relation to saturated granular soils. However, in relation to clayey soils, the WSI showed values less than ε^* and frequently negative. This behavior is corroborated by literature regarding correlations between body wave velocity and lithology, in relation to the dry and saturated condition.

In conclusion, this study highlighted that the WSI is more susceptible to lithology and the unsaturated–saturated transition layer than to the V_P/V_S and Poisson's ratio.

Acknowledgments

The research was supported by COFIN 2005 project (prot. 2003049828_002, resp. F. M. Guadagno). We are very grateful to Soheil Nazarian for his comments and suggestions, and scientific supports. We also thank an anonymous reviewer for careful review. Finally, we are grateful to R. Bruno, L. Nardone and G. Pasquale for the useful support in the field tests.

References

Ackerman, H.D., Pankratz, L.W., Dansereau, D., 1986. Resolution of ambiguities of seismic refraction traveltime curves. Geophysics 51, 223–235.
Azaria, A., Zelt, C.A., Levander, A., 2003. High-resolution seismic mapping at a groundwater contamination site: 3-D traveltime tomography of refraction data. EGS–AGU–EUG joint Assembly, Abstracts from the meeting held in Nice.
Bachrach, R., Nur, A., 1998. High-resolution shallow-seismic experiments in sand, Part I: water table, fluid flow and saturation. Geophysics 63 (4), 1225–1233.
Biot, M.A., 1956a. Theory of propagation of elastic waves in fluid-saturated porous solid. Part I: higher frequency range. Journal of Acoustic Society of America 28, 168–178.
Biot, M.A., 1956b. Theory of propagation of elastic waves in fluid-saturated porous solid. Part II: higher frequency range. Journal of Acoustic Society of America 28, 179–191.
Biot, M.A., 1962. Mechanism of deformation and acoustic propagation in porous media. Journal of Applied Geophysics 33, 1482–1498.
Castagna, J.P., Batzle, M.L., Eastwood, R.L., 1985. Relationship between compressional-wave and shear-wave velocities in clastic silicate rocks. Geophysics 50 (4), 571–581.
Foti, S., Lai, C.G., Lancellotta, R., 2002. Porosity of fluid-saturated porous media from measured seismic wave velocities. Geotechnique 52 (5), 359–373.
Giocoli, A. et al., in press. Electrical resistivity tomography investigations in the Ufita valley (Southern Italy). Annals of Geophysics.
Haeni, F.P., 1986. Application of seismic refraction methods in groundwater modelling studies in New England. Geophysics 51 (2), 236–249.
Haeni, F.P., 1988. Application of seismic-refraction techniques to hydrologic studies. U.S. Geological Survey Techniques of Water-Resources Investigations, book 2, chap. D2. 86 p.
Hasbrouk, W.P., 1987. Hammer-impact, shear-wave studies. In: Danbom, S.H., Domenico, S.N. (Eds.), Shear-wave exploration: Geophysical development series. Soc. Expl. Geophys., Vol. 1, pp. 97–121.
Hasselstroem, B., 1969. Water prospecting and rock-investigation by the seismic refraction method. Geoexploration 7 (2), 213.
Ivanov, J., Richard, D., Miller, R.D., Xia, J., Steeples, D., 2005. The inverse problem of refraction travel times, Part II: quantifying refraction nonuniqueness using a three-layer model. Pure applied geophysicsn 162, 461–477.
Lawton, C., 1990. Component refraction seismic experiment. Canadian Journal of Exploration Geophysics 26 (1&2), 7–16.
Lees, J.M., Wu, H., 2000. Poisson's ratio and porosity at Coso geothermal area, California. Journal of volcanology and geothermal research 95, 157–173.
Nicholson, C., Simposon, D.W., 1985. Changes in V_P/V_s with depth: implication for appropriate velocity models, improved earthquake locations, and material properties of the upper crust. Bulletin of the Seismological Society of America 75, 1105–1124.
Qin, F., Luo, Y., Olsen, K., Cai, W., Schuster, G.T., 1992. Finite-difference solution of the eikonal equation. Geophysics 57, 478–487.
Sander, J.E., 1978. The blind zone in seismic ground-water exploration. Ground Water 165, 394–395.
Schuter, G.T., Quintus-Bosz, A., 1993. Wavepath Eikonal Traveltime Inversion: theory. Geophysics 58 (9), 1314–1323.
Stümpel, H., Kähler, S., Meissner, R., Milkereit, B., 1984. The use of seismic shear waves and compressional waves for lithological problems of shallow sediments. Geophysical Prospecting 32, 662–675.
Watson, D.B., Doll, W.E., Jeffrey Gamey, T., Sheehan, J.R., Jardine, P.M., 2005. Plume and lithologic profiling with surface resistivity and seismic tomography. Ground Water 43 (2), 169–177.
Yoshimi, Y., Tanaka, K., Tokimatsu, K., 1989. Liquefaction resistance of a partially saturated sand. Soils Foundation 29, 157–162.
Zelt, A.C., Azaria, A., Levander, A., 2006. 3D seismic refraction traveltime tomography at a groundwater contamination site. Geophysics 58 (9), 1314–1323.
Zohdy, A.A.R., Eaton, G.P., Mabey, D.R., 1974. Application of surface geophysics to groundwater investigation. U.S. Geol. Surv. Techniques of Water-Resource Investigations, book 2, chapter D1.

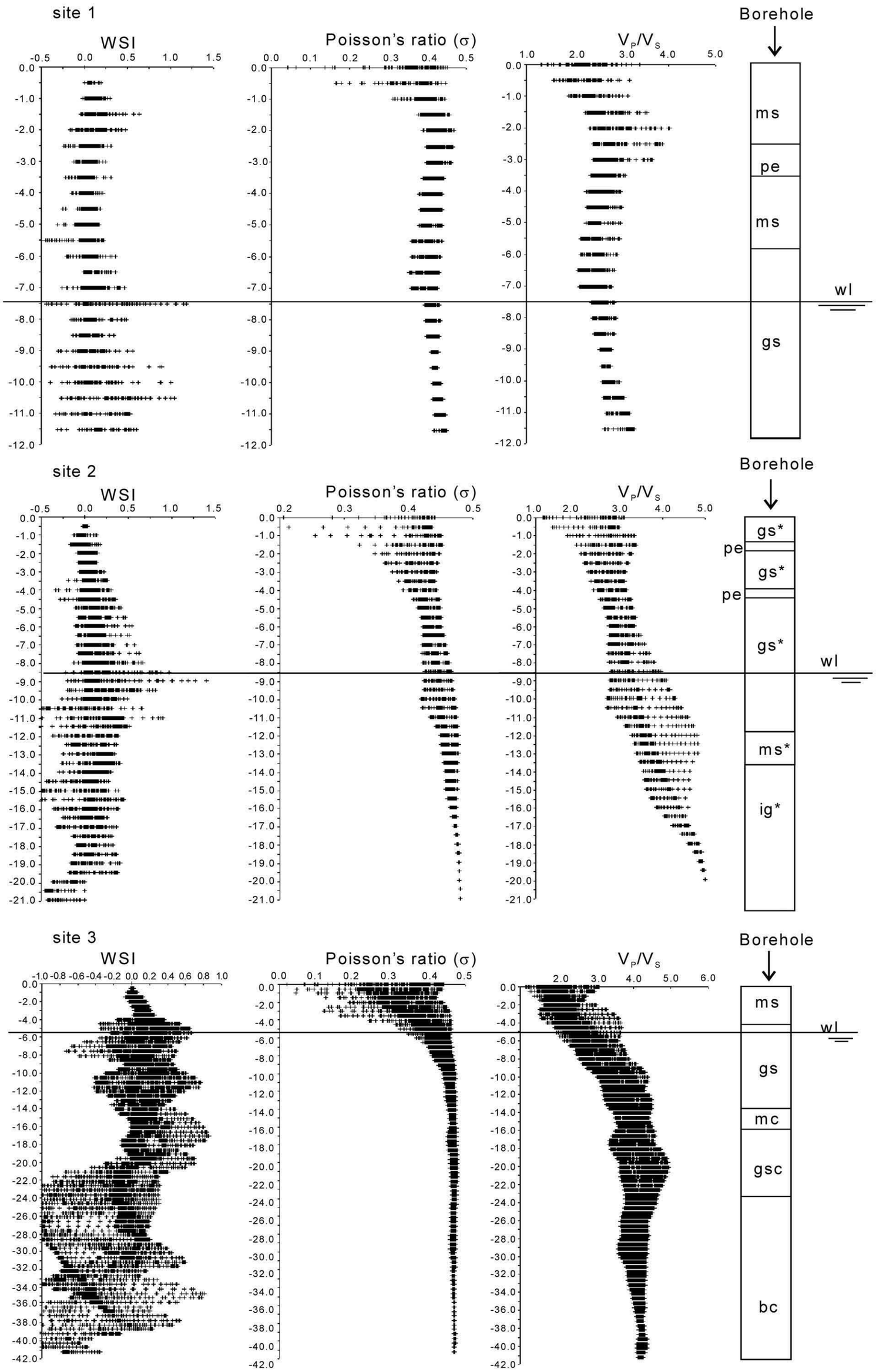

Fig. 16. Comparison among WSI, Poisson's ratio (σ) and V_P/V_S in relation to the lithology sequences (for soil suffixes see Fig. 6).